
Deep Complex Networks

Chiheb Trabelsi^{*}
 MILA, Université de Montréal
 Polytechnique Montréal
 chiheb.trabelsi@polymtl.ca

Olexa Bilaniuk^{*}
 MILA, Université de Montréal
 olexa.bilaniuk@umontreal.ca

Dmitriy Serdyuk[†]
 MILA, Université de Montréal
 serdyuk@iro.umontreal.ca

Sandeep Subramanian[†]
 MILA, Université de Montréal
 sandeep.subramanian.1
 @umontreal.ca

João Felipe Santos
 INRS-EMT
 jfsantos@emt.inrs.ca

Soroush Mehri
 Microsoft Maluuba
 soroush.mehri@microsoft.com

Negar Rostamzadeh
 Element AI
 negar@elementai.com

Yoshua Bengio[‡]
 MILA, Université de Montréal
 find.me@the.web

Christopher J Pal
 MILA, Université de Montréal
 Polytechnique Montréal
 christopher.pal@polymtl.ca

Abstract

At present, the vast majority of building blocks, techniques, and architectures for deep learning are based on real-valued operations and representations. However, recent work on recurrent neural networks and older fundamental theoretical analysis suggests that complex numbers could have a richer representational capacity and could also facilitate noise-robust memory retrieval mechanisms. Despite their attractive properties and potential for opening up entirely new neural architectures, complex-valued deep neural networks have been marginalized due to the absence of the building blocks required to design such models. In this work, we provide the key atomic components for complex-valued deep neural networks and apply them to convolutional feed-forward networks. More precisely, we rely on complex convolutions and present algorithms for complex batch-normalization, complex weight initialization strategies for complex-valued neural nets and we use them in experiments with end-to-end training schemes. We demonstrate that such complex-valued models are able to achieve comparable or better performance than their real-valued counterparts. We test deep complex models on several computer vision tasks and on music transcription using the MusicNet dataset where we achieve state of the art performance.

^{*}Equal first author

[†]Equal contributions

[‡]CIFAR Senior Fellow

1 Introduction

Recent research advances have made significant progress in addressing the difficulties involved in learning deep neural network architectures. Key innovations include normalization techniques [Ioffe and Szegedy, 2015, Salimans and Kingma, 2016] and the emergence of gating-based feed-forward neural networks like Highway Networks [Srivastava et al., 2015]. Residual networks [He et al., 2015a, 2016] have emerged as one of the most popular and effective strategies for training very deep convolutional neural networks (CNNs). Both highway networks and residual networks facilitate the training of deep networks by providing shortcut paths for easy gradient flow to lower network layers thereby diminishing the effects of vanishing gradients [Hochreiter, 1991]. He et al. [2016] show that learning explicit residuals of layers helps in avoiding the vanishing gradient problem and provides the network with an easier optimization problem. Batch normalization [Ioffe and Szegedy, 2015] demonstrates that standardizing the activations of intermediate layers in a network across a minibatch acts as a powerful regularizer as well as providing faster training and better convergence properties. Further, such techniques that standardize layer outputs become critical in deep architectures due to the vanishing and exploding gradient problems.

The role of representations based on complex numbers has started to receive increased attention, due to their potential to enable easier optimization [Nitta, 2002], better generalization characteristics [Hirose and Yoshida, 2012], faster learning [Arjovsky et al., 2015, Danihelka et al., 2016, Wisdom et al., 2016] and to allow for noise-robust memory mechanisms [Danihelka et al., 2016]. Wisdom et al. [2016] and Arjovsky et al. [2015] show that using complex numbers in recurrent neural networks (RNNs) allows the network to have a richer representational capacity. Danihelka et al. [2016] present an LSTM [Hochreiter and Schmidhuber, 1997] architecture augmented with associative memory with complex-valued internal representations. Their work highlights the advantages of using complex-valued representations with respect to retrieval and insertion into an associative memory. In residual networks, the output of each block is added to the output history accumulated by summation until that point. An efficient retrieval mechanism could help to extract useful information and process it within the block.

In order to exploit the advantages offered by complex representations, we present a general formulation for the building components of complex-valued deep neural networks and apply it to the context of feed-forward convolutional networks. Our contributions in this paper are as follows:

1. A formulation of complex batch normalization, which is described in Section 3.4;
2. Complex weight initialization, which is presented in Section 3.5;
3. The state of the art result on a multi-instrument music transcription dataset (MusicNet), presented in Section 4.2 .

We demonstrate the effectiveness of deep complex networks on three standard image classification benchmarks⁴ – CIFAR-10, CIFAR-100, Street View House Numbers (SVHN), and a music transcription task on the MusicNet dataset. The results obtained for vision classification tasks show that learning complex-valued representations results in performance that is competitive with the respective real-valued architectures. Our promising results in music transcription open up to new horizons for deep complex-valued neural networks applied on acoustic related tasks.

We continue this paper with discussion of motivation for using complex operations and related work.

2 Motivation and Related Work

Using complex parameters has numerous advantageous from computational, biological, and signal processing perspectives.

From a computational point of view, it has been shown in Danihelka et al. [2016] that Holographic Reduced Representations [Plate, 2003], which use complex numbers, are numerically efficient and stable in the context of information retrieval from an associative memory. Danihelka et al. [2016] insert key-value pairs in the associative memory by addition into a *memory trace*. Although not typically viewed as such, residual networks [He et al., 2015a, 2016] and Highway Networks [Srivastava

⁴The source code is located at http://github.com/ChihebTrabelsi/deep_complex_networks

et al., 2015] have a similar architecture to associative memories: each ResNet residual path computes a residual that is then inserted – by summing into the “memory” provided by the identity connection. Given residual networks’ resounding success on several benchmarks and their functional similarity to associative memories, it seems interesting to marry both together. This motivates us to incorporate complex weights and activations in residual networks. Together, they offer a mechanism by which useful information may be retrieved, processed and inserted in each residual block.

Orthogonal weight matrices, whose eigenvalues have modulus 1, provide a novel angle of attack on the well-known vanishing and exploding gradient problems in RNNs. Unitary RNNs [Arjovsky et al., 2015] are based on unitary weight matrices, which are a complex generalization of orthogonal weight matrices. Compared to their orthogonal counterparts, unitary matrices provide a richer representation, for instance being capable of implementing the discrete Fourier transform, and thus of discovering spectral representations. Arjovsky et al. [2015] show the potential of this type of recurrent neural networks on toy tasks. Wisdom et al. [2016] provided a more general framework for learning unitary matrices and they applied their method on toy tasks and on a real-world speech task.

Using complex weights in neural networks also has biological motivation. Reichert and Serre [2013] have proposed a biologically plausible deep network that allows one to construct richer and more versatile representations using complex-valued neuronal units. The complex-valued formulation allows one to express the neuron’s output in terms of its firing rate and the relative timing of its activity. The amplitude of the complex neuron represents the former and its phase the latter. Input neurons that have similar phases are called *synchronous* as they add constructively, whereas *asynchronous* neurons add destructively and thus interfere with each other. This is related to the gating mechanism used in both deep feed-forward neural networks [Srivastava et al., 2015, van den Oord et al., 2016a,b] and recurrent neural networks [Hochreiter and Schmidhuber, 1997, Cho et al., 2014, Zilly et al., 2016] as this mechanism learns to synchronize inputs that the network propagates at a given feed-forward layer or time step. In the context of deep gating-based networks, synchronization means the propagation of inputs whose controlling gates simultaneously hold high values. These controlling gates are usually the activations of a sigmoid function. This ability to take into account phase information might explain the effectiveness of incorporating complex-valued representations in the context of recurrent neural networks.

The phase component is not only important from a biological point of view but also from a signal processing perspective. It has been shown that the phase information in speech signals affects their intelligibility [Shi et al., 2006]. Oppenheim and Lim [1981] show that the amount of information present in the phase of an image is sufficient to recover the majority of the information encoded in its magnitude. In fact, phase provides a detailed description of objects as it encodes shapes, edges, and orientations.

Recently, Rippel et al. [2015] leveraged the Fourier spectral representation for convolutional neural networks, providing a technique for parameterizing convolution kernel weights in the spectral domain, and performing pooling on the spectral representation of the signal. However, the authors avoid performing complex-valued convolutions, instead building from real-valued kernels in the spatial domain. In order to ensure that a complex parametrization in the spectral domain maps onto real-valued kernels, the authors impose a conjugate symmetry constraint on the spectral-domain weights, such that when the *inverse Fourier transform* is applied to them, it only yields real-valued kernels.

As pointed out in Reichert and Serre [2013], the use of complex-valued neural networks [Georgiou and Koutsougeras, 1992, Zemel et al., 1995, Kim and Adali, 2003, Hirose, 2003, Nitta, 2004] has been investigated long before the earliest deep learning breakthroughs [Hinton et al., 2006, Bengio et al., 2007, Poultney et al., 2007]. Recently Reichert and Serre [2013], Bruna et al. [2015], Arjovsky et al. [2015], Danihelka et al. [2016], Wisdom et al. [2016] have tried to bring more attention to the usefulness of deep complex neural networks by providing theoretical and mathematical motivation for using complex-valued deep networks. However, to the best of our knowledge, most of the recent works using complex valued networks have been applied on toy tasks, with the exception of some attempts such in Oyallon and Mallat [2015], Tygert et al. [2015] who reported results on CIFAR-10. Wisdom et al. [2016] have also performed a real-world speech task consisting of predicting the log magnitude of the future *short time Fourier transform* frames. Much remains to be done

to develop proper tools and a general framework for training deep neural networks with complex-valued parameters.

Given the compelling reasons for using complex-valued representations, the absence of such frameworks represents a gap in machine learning tooling, which we fill by providing a set of building blocks for deep complex-valued neural networks that enable them to perform similarly to, or better than, their real-valued counterparts on real-world tasks.

3 Complex Building Blocks

In this section, we present the core of our work, laying down the mathematical framework for implementing complex-valued building blocks of a deep neural network.

3.1 Representation of Complex Numbers

We start by outlining the way in which complex numbers are represented in our framework. A complex number $z = a + ib$ has a real component a and an imaginary component b . We represent the real part a and the imaginary part b of a complex number as logically distinct real valued entities and simulate complex arithmetic using real-valued arithmetic internally. Consider a typical real-valued 2D convolution layer that has N feature maps such that N is divisible by 2; to represent these as complex numbers, we allocate the *first* $N/2$ feature maps to represent the real components and the remaining $N/2$ to represent the imaginary ones. Thus, for a four dimensional weight tensor W that links N_{in} input feature maps to N_{out} output feature maps and whose kernel size is $m \times m$ we would have a weight tensor of size $(N_{out} \times N_{in} \times m \times m)/2$ complex weights.

3.2 Complex Convolution

In order to perform the equivalent of a traditional real-valued 2D convolution in the complex domain, we convolve a complex filter matrix $\mathbf{W} = \mathbf{A} + i\mathbf{B}$ by a complex vector $\mathbf{h} = \mathbf{x} + i\mathbf{y}$ where \mathbf{A} and \mathbf{B} are real matrices and \mathbf{x} and \mathbf{y} are real vectors since we are simulating complex arithmetic using real-valued entities. As the convolution operator is distributive, convolving the vector \mathbf{h} by the filter \mathbf{W} we obtain:

$$\mathbf{W} * \mathbf{h} = (\mathbf{A} * \mathbf{x} - \mathbf{B} * \mathbf{y}) + i(\mathbf{B} * \mathbf{x} + \mathbf{A} * \mathbf{y}). \quad (1)$$

If we use matrix notation to represent real and imaginary parts of the convolution operation we have:

$$\begin{bmatrix} \Re(\mathbf{W} * \mathbf{h}) \\ \Im(\mathbf{W} * \mathbf{h}) \end{bmatrix} = \begin{bmatrix} \mathbf{A} & -\mathbf{B} \\ \mathbf{B} & \mathbf{A} \end{bmatrix} * \begin{bmatrix} \mathbf{x} \\ \mathbf{y} \end{bmatrix}. \quad (2)$$

This is illustrated in 1a

3.3 Depth and Width in Deep Complex Networks

In this section, we show that for a given parameter budget, the complex feed-forward architecture can go wider and deeper than its real counterpart.

For simplicity let us assume that we have a deep feed-forward network which has N units at each layer and whose depth is L . For a complex feed-forward network, this would be equivalent of having $N/2$ complex units at each layer. For a given layer, the number of parameters for each of the real and imaginary weights would be equal to $N/2 \times N/2$ which means $N^2/2$ when we sum both. On the other hand, for a real-valued feed-forward network, the total number of parameters for a given layer would be equal to N^2 . We can see that the complex-valued architecture allows one to halve the number of total weights and so to go wider than its real counterpart for a given parameter configuration. The number of total complex parameters for the whole network would be $(N^2/2)^L = (N/\sqrt{2})^{2L}$. For the real-valued counterpart, the number of parameters would be equal to $(N)^{2L}$. We can clearly see that for a given width and depth, the number of parameters in the real-valued neural network is $(\sqrt{2})^{2L}$ more than the complex-valued one. This means that a complex architecture could exploit depth exponentially better than its real counterpart as it can be exponentially deeper for a given budget of parameters.

3.4 Complex Batch Normalization

Deep networks generally rely upon Batch Normalization [Ioffe and Szegedy, 2015] to accelerate learning. In some cases batch normalization is essential to optimize the model. The standard formulation of Batch Normalization applies only to real values. In this section, we propose a batch normalization formulation that can be applied for complex-values.

To standardize an array of complex numbers to the standard normal complex distribution, it is not sufficient to translate and scale them such that their mean is 0 and their variance 1. This type of normalization does not ensure equal variance in both the real and imaginary components, and the resulting distribution could be very eccentric.

We instead choose to treat this problem as one of whitening 2D vectors, which implies scaling the data by the square root of their variances along each of the two principal components. This can be done by multiplying the 0-centered data $(\mathbf{x} - \mathbb{E}[\mathbf{x}])$ by the inverse square root of the 2×2 covariance matrix \mathbf{V} :

$$\tilde{\mathbf{x}} = (\mathbf{V})^{-\frac{1}{2}} (\mathbf{x} - \mathbb{E}[\mathbf{x}]),$$

where the covariance matrix \mathbf{V} is

$$\mathbf{V} = \begin{pmatrix} V_{rr} & V_{ri} \\ V_{ir} & V_{ii} \end{pmatrix} = \begin{pmatrix} \text{Cov}(\Re\{\mathbf{x}\}, \Re\{\mathbf{x}\}) & \text{Cov}(\Re\{\mathbf{x}\}, \Im\{\mathbf{x}\}) \\ \text{Cov}(\Im\{\mathbf{x}\}, \Re\{\mathbf{x}\}) & \text{Cov}(\Im\{\mathbf{x}\}, \Im\{\mathbf{x}\}) \end{pmatrix}.$$

The square root and inverse of 2×2 matrices has an inexpensive, analytical solution, and its existence is guaranteed by the positive (semi-)definiteness of \mathbf{V} . Positive definiteness of \mathbf{V} is ensured by the addition of $\epsilon \mathbf{I}$ to \mathbf{V} a Tikhonov regularizer. The mean subtraction and multiplication by the inverse square root of the variance ensures that $\tilde{\mathbf{x}}$ has standard complex distribution with mean $\mu = 0$, covariance $\Gamma = 1$ and pseudo-covariance (also called relation) $C = 0$. The mean, the covariance and the pseudo-covariance are given by:

$$\begin{aligned} \mu &= \mathbb{E}[\tilde{\mathbf{x}}] \\ \Gamma &= \mathbb{E}[(\tilde{\mathbf{x}} - \mu)(\tilde{\mathbf{x}} - \mu)^*] = V_{rr} + V_{ii} + i(V_{ir} - V_{ri}) \\ C &= \mathbb{E}[(\tilde{\mathbf{x}} - \mu)(\tilde{\mathbf{x}} - \mu)] = V_{rr} - V_{ii} + i(V_{ir} + V_{ri}). \end{aligned} \tag{3}$$

The normalization procedure allows one to decorrelate the imaginary and real parts of a unit. This has the advantage of avoiding co-adaptation between the two components which reduces the risk of overfitting [Cogswell et al., 2015, Srivastava et al., 2014].

Analogously to the real-valued batch normalization algorithm, we use two parameters, β and γ . The shift parameter β is a complex parameter with two learnable components (the real and imaginary means). The scaling parameter γ is a 2×2 positive semi-definite matrix with only three degrees of freedom, and thus only three learnable components. In much the same way that the matrix $(\mathbf{V})^{-\frac{1}{2}}$ normalized the variance of the input to 1 along both of its original principal components, so does γ scale the input along desired new principal components to achieve a desired variance. The scaling parameter γ is given by:

$$\gamma = \begin{pmatrix} \gamma_{rr} & \gamma_{ri} \\ \gamma_{ri} & \gamma_{ii} \end{pmatrix}.$$

As the normalized input $\tilde{\mathbf{x}}$ has real and imaginary variance 1, we initialize both γ_{rr} and γ_{ii} to $1/\sqrt{2}$ in order to obtain a modulus of 1 for the variance of the normalized value. γ_{ri} , $\Re\{\beta\}$ and $\Im\{\beta\}$ are initialized to 0. The complex batch normalization is defined as:

$$\text{BN}(\mathbf{x}) = \gamma \tilde{\mathbf{x}} + \beta. \tag{4}$$

We use running averages with momentum to maintain an estimate of the complex batch normalization statistics during training and testing. The moving averages of V_{ri} and β are initialized to 0. The moving averages of V_{rr} and V_{ii} are initialized to $1/\sqrt{2}$. The momentum for the moving averages is set to 0.9.

3.5 Complex Weight Initialization

In a general case, particularly when batch normalization is not performed, proper initialization is critical in reducing the risks of vanishing or exploding gradients. To do this, we follow the same

steps as in Glorot and Bengio [2010] and He et al. [2015b] to derive the variance of the complex weight parameters.

A complex weight has a polar form as well as a rectangular form

$$W = |W|e^{i\theta} = \Re\{W\} + i\Im\{W\}, \quad (5)$$

where θ and $|W|$ are respectively the argument (phase) and magnitude of W .

Variance is the difference between the *expectation of the squared magnitude* and the *square of the expectation*:

$$\text{Var}(W) = \mathbb{E}[WW^*] - (\mathbb{E}[W])^2 = \mathbb{E}[|W|^2] - (\mathbb{E}[W])^2,$$

which reduces, in the case of W symmetrically distributed around 0, to $\mathbb{E}[|W|^2]$. We do not know yet the value of $\text{Var}(W) = \mathbb{E}[|W|^2]$. However, we do know a related quantity, $\text{Var}(|W|)$, because the magnitude of complex normal values, $|W|$, follows the Rayleigh distribution (Chi-distributed with two degrees of freedom (DOFs)). This quantity is

$$\text{Var}(|W|) = \mathbb{E}[|W||W|^*] - (\mathbb{E}[|W|])^2 = \mathbb{E}[|W|^2] - (\mathbb{E}[|W|])^2. \quad (6)$$

Putting them together:

$$\text{Var}(|W|) = \text{Var}(W) - (\mathbb{E}[|W|])^2, \text{ and } \text{Var}(W) = \text{Var}(|W|) + (\mathbb{E}[|W|])^2.$$

We now have a formulation for the variance of W in terms of the variance and expectation of its magnitude, both properties analytically computable from the Rayleigh distribution's single parameter, σ , indicating the *mode*. These are:

$$\mathbb{E}[|W|] = \sigma \sqrt{\frac{\pi}{2}}, \quad \text{Var}(|W|) = \frac{4 - \pi}{2} \sigma^2.$$

The variance of W can thus be expressed in terms of its generating Rayleigh distribution's single parameter, σ , thus:

$$\text{Var}(W) = \frac{4 - \pi}{2} \sigma^2 + \left(\sigma \sqrt{\frac{\pi}{2}} \right)^2 = 2\sigma^2. \quad (7)$$

If we want to respect the Glorot and Bengio [2010] criterion which ensures that the variances of the input, the output and their gradients are the same, then we would have $\text{Var}(W) = 2/(n_{in} + n_{out})$, where n_{in} and n_{out} are the number of input and output units respectively. In such case, $\sigma = 1/\sqrt{n_{in} + n_{out}}$. If we want to respect the He et al. [2015b] initialization that presents an initialization criterion that is specific to ReLUs, then $\text{Var}(W) = 2/n_{in}$ which $\sigma = 1/\sqrt{n_{in}}$.

The magnitude of the complex parameter W is then initialized using the Rayleigh distribution with the appropriate mode σ . We can see from equation 7, that the variance of W depends on its magnitude and not on its phase. We then initialize the phase using the uniform distribution between $-\pi$ and π . By performing the multiplication of the magnitude by the phasor as is detailed in equation 5, we perform the complete initialization of the complex parameter.

We explore in the experimental setup another variant of initialization that leverages the independence property of unitary matrices. As it is stated in Cogswell et al. [2015], Srivastava et al. [2014], and Tompson et al. [2015], learning decorrelated features is beneficial for learning as it allows to perform better generalization and faster learning. This motivates us to achieve initialization by considering a (semi-)unitary matrix which is reshaped to the size of the weight tensor. Once this is done, the weight tensor is multiplied by $\sqrt{H_{var}/\text{Var}(W)}$ or $\sqrt{Glorot_{var}/\text{Var}(W)}$ where $Glorot_{var}$ and H_{var} are respectively equal to $2/(n_{in} + n_{out})$ and $2/n_{in}$. In such a way we allow kernels to be independent from each other as much as possible while respecting the desired criterion.

3.6 Complex Convolutional Residual Network

A deep convolutional residual network of the nature presented in He et al. [2015a, 2016] consists of three *stages* within which feature maps maintain the same shape. At the end of a stage, the feature maps are downsampled by a factor of 2 and the number of convolution filters is doubled. The sizes of the convolution kernels are always set to 3×3 . Within a stage, there are several *residual blocks* which comprise 2 convolution layers each. The contents of one such residual block in the real and complex setting is illustrated in 1b.

Table 1: Model Architecture. S1, S2 and S3 filters are the number of convolution filters used in each layer in stages 1, 2 and 3. (S) denotes a small network while (L) denotes a large network.

ARCHITECTURE	PARAMS	LAYERS	S1 FILTERS	S2 FILTERS	S3 FILTERS
REAL (S)	860K	56	16	32	64
COMPLEX (S)	860K	64	22	44	88
REAL (L)	1.71M	110	16	32	64
COMPLEX (L)	1.70M	118	22	44	88

Table 2: Classification error on CIFAR-10, CIFAR-100 and SVHN. Note that He et al. [2016] uses a 110 layer model.

ARCHITECTURE	CIFAR-10	CIFAR-100	SVHN
REAL (S)	6.22	28.43	3.54
COMPLEX (S)	6.15	28.60	3.79
REAL (L)	5.98	26.74	3.41
COMPLEX (L)	5.60	27.09	3.30
HE ET AL. [2016] ⁵	6.37	—	—

In the complex valued setting, the majority of the architecture remains identical to the one presented in He et al. [2016] with a few subtle differences. Since all datasets that we work with are real-valued, we present a way to learn their imaginary components to let the rest of the network operate in the complex plane. We learn the initial imaginary component of our input by performing the operations present within a single real-valued residual block

$$BN \rightarrow ReLU \rightarrow Conv \rightarrow BN \rightarrow ReLU \rightarrow Conv$$

The parameters of this real-valued residual block are trained by backpropagating errors from the task specific loss function. Secondly, we perform a $Conv \rightarrow BN \rightarrow ReLU$ operation on the obtained complex input before feeding it to the first residual block. We also perform the same operation on the real-valued network input instead of $Conv \rightarrow Maxpooling$ as in He et al. [2016]. Inside, residual blocks, we subtly alter the way in which we perform a projection at the end of a stage in our network. We concatenate the output of the last residual block with the output of a 1x1 convolution applied on it with the same number of filters used throughout the stage and subsample by a factor of 2. In contrast, He et al. [2016] perform a similar 1x1 convolution with twice the number of feature filters in the current stage to both downsample the feature maps spatially and double them in number.

4 Experimental Results

In this section, we present empirical results from using our model to perform image and music classification. First, we present our model’s architecture followed by the results we obtained on three standard image classification benchmarks – CIFAR-10, CIFAR-100, and SVHN as well as the results on automatic music transcription on the MusicNet benchmark.

4.1 Image Recognition

As briefly discussed in section 3.6, we adopt an architecture that is similar to He et al. [2016]. This will also serve as our baseline to compare against. The internal differences between our models are also discussed in 3.6. We train real and complex-valued networks of two different sizes – a small network of ~860k parameters and a large network with ~1.7M parameters, denoted by (S) and (L) respectively in table 2. S1 filters, S2 filters and S3 filters refer to the number of convolution filters used in each convolution layer in stages 1, 2 and 3 respectively. As pointed out in section 3.3, our complex network has fewer parameters than an identical real-valued one. We therefore alter the number of residual blocks per stage and the number of filters of each convolutional layer within a stage to appropriately to make the number of parameters equal to that of its real valued counterpart as detailed in table 1.

⁵110 layer network (Table 2 of He et al. [2016])

Both real and complex-valued networks have 3 stages within which the number and shape of feature maps and convolution kernels are preserved. At the end of each stage the feature maps are spatially downsampled linearly by a factor of 2 with a convolution and the number of convolution kernels are doubled thereby doubling the number of feature maps as well. A global average pooling layer followed by a single fully connected layer with a softmax function is used to classify the input as belonging to one of 10 classes in the CIFAR-10 and SVHN datasets and 100 classes for CIFAR-100.

All models (real and complex) were trained using the backpropagation algorithm with Stochastic Gradient Descent with Nesterov momentum [Nesterov, 1983] set at 0.9. We also clip the norm of our gradients to 1. We tweaked the learning rate schedule used in He et al. [2016] in both the real and complex residual networks to extract small performance improvements in both. We start our learning rate at 0.01 for the first 10 epochs to warm up the training and then set it at 0.1 from epoch 10-100 and then anneal the learning rates by a factor of 10 at epochs 120 and 150.

Table 2 presents our results on performing image classification on CIFAR-10, CIFAR-100 and SVHN. For computational reasons, we train only on a subset of 73,257 images on SVHN but still test on all 26,032 images. As described in sections 4.1 and 3.6, we have a real and complex valued network of two different sizes. The effect of model size is consistent with the observations presented in He et al. [2016], Zagoruyko and Komodakis [2016] which show that increasing model capacity helps in reducing both training as well as testing error. Our large complex model outperforms the real-valued variant on CIFAR-10 and SVHN and our smaller complex model outperforms the real-valued one on CIFAR-10. We can also observe in 2 that the complex network’s training curve is more stable in the initial few epochs and decreases faster.

Feature maps in our network are visualized in Figures 3, and 4. Figure 3 contains plots of feature maps (left) and their polar representations (right) in the last convolution layer of the first stage of the network. Figure 4 presents just feature maps of the last convolution layer in stages 2 (left) and 3 (right). Different rows correspond to different inputs (first column) that are fed to the network to generate feature maps. For each input, feature maps are plotted as 3 sets of (real, imaginary) pairs with the real component and its corresponding imaginary component adjacent to each other starting with a real feature map. The feature maps appear to learn spatially complimentary heatmaps.

4.2 Automatic Music Transcription on MusicNet Dataset

In this section we present results for the automatic music transcription (AMT) task. The nature of an audio signal allows one to exploit complex operations as presented earlier in the paper. The experiments were performed on the MusicNet dataset [Thickstun et al., 2016]. For computational efficiency we resampled the original input from 44.1kHz to 11kHz using the algorithm described in Smith [2002]. This sampling rate is sufficient to recognize frequencies presented in the dataset while reducing computational cost dramatically. We modeled each of the 84 notes that are present in the dataset with independent sigmoids. As in the baseline, we performed experiments on the raw signal and the frequency spectrum. For complex experiments with the raw signal, we considered its imaginary part equal to zero. When using the spectrum input we used its complex representation (instead of only the magnitudes, as usual for AMT) for both real and complex models. For the real model, we considered the real and imaginary components of the spectrum as separate channels. The model we used for raw signals is a shallow convolutional network similar to the model used in the baseline, with the size reduced by a factor of 4 (corresponding to the reduction of the sampling rate). The filter size was 512 samples (about 12ms) with a stride of 16. The model for the spectral input is similar to the VGG model [Simonyan and Zisserman, 2015]. The first layer has filter with size of 7 and is followed by 5 convolutional layers with filters of size 3. In all of our experiments we use an input window of 4096 samples or its corresponding FFT (which corresponds to the 16,384 window used in the baseline) and predicted notes in the center of the window.

The complex network was initialized using the unitary initialization scheme respecting the He criterion as described in Section 3.5. For the real-valued network, we have used the analogue initialization of the weight tensor. It consists of performing an orthogonal initialization with a gain of $\sqrt{2}$. The complex batch normalization was applied according to Section 3.4. Following Thickstun et al. [2016] we used recordings with ids ‘2303’, ‘2382’, ‘1819’ as the test subset and additionally we created a validation subset using recording ids ‘2131’, ‘2384’, ‘1792’, ‘2514’, ‘2567’, ‘1876’ (randomly chosen from the training set). The validation subset was used for model selection and early stopping. The remaining 321 files were used for training. The results are summarized on Table 3.

Table 3: MusicNet experiments. *FS* is the sampling rate. *Params* is the total number of parameters. We report the average precision (AP) metric that is the area under the precision-recall curve.

ARCHITECTURE	FS	PARAMS	AP, %
SHALLOW, REAL	11KHZ		66.1
SHALLOW, COMPLEX	11KHZ		66.0
SHALLOW, THICKSTUN ET AL. [2016]	44.1KHZ	-	67.8
DEEP, REAL	11KHZ	10.0M	69.6
DEEP, COMPLEX	11KHZ	8.8M	72.9

We achieve a performance comparable to the baseline with the shallow convolutional network. The deep complex convolutional network, which has significantly less parameters than the real model, achieves 72.9% average precision which is the state of the art to the best of our knowledge. See the Appendix for precision-recall curves and a sample of the output of the model.

5 Conclusions

We have presented key building blocks required to train complex valued neural networks, such as complex batch normalization and complex weight initialization. We have also explored some complex convolutional network architectures which have yielded competitive results for image classification and state of the art results for a music transcription task. We anticipate our work will open the doors to further investigation of complex valued networks for deep learning models and their application to more challenging tasks such as generative models for audio and images.

Acknowledgements

We are grateful to all students at MILA, especially Jason Jo and Anna Huang for helpful feedback and discussions. We thank Jesse Engel for valuable conversations. We also thank the developers of Theano [Theano Development Team, 2016] and Keras [Chollet et al., 2015]. We are grateful to Samsung and the Fonds de Recherche du Québec – Nature et Technologie for their financial support. We would also like to acknowledge NVIDIA for donating a DGX-1 computer used in this work.

References

Sergey Ioffe and Christian Szegedy. Batch normalization: Accelerating deep network training by reducing internal covariate shift. *arXiv preprint arXiv:1502.03167*, 2015.

Tim Salimans and Diederik P Kingma. Weight normalization: A simple reparameterization to accelerate training of deep neural networks. *arXiv preprint arXiv:1602.07868*, 2016.

Rupesh K Srivastava, Klaus Greff, and Jürgen Schmidhuber. Training very deep networks. In *Advances in neural information processing systems*, pages 2377–2385, 2015.

Kaiming He, Xiangyu Zhang, Shaoqing Ren, and Jian Sun. Deep residual learning for image recognition. *arXiv preprint arXiv:1512.03385*, 2015a.

Kaiming He, Xiangyu Zhang, Shaoqing Ren, and Jian Sun. Identity mappings in deep residual networks. *arXiv preprint arXiv:1603.05027*, 2016.

Sepp Hochreiter. *Untersuchungen zu dynamischen neuronalen Netzen*. PhD thesis, diploma thesis, institut für informatik, lehrstuhl prof. brauer, technische universität münchen, 1991.

T Nitta. On the critical points of the complex-valued neural network. In *Neural Information Processing, 2002. ICONIP'02. Proceedings of the 9th International Conference on*, volume 3, pages 1099–1103. IEEE, 2002.

Akira Hirose and Shotaro Yoshida. Generalization characteristics of complex-valued feedforward neural networks in relation to signal coherence. *IEEE Transactions on Neural Networks and learning systems*, 23(4): 541–551, 2012.

Martin Arjovsky, Amar Shah, and Yoshua Bengio. Unitary evolution recurrent neural networks. *arXiv preprint arXiv:1511.06464*, 2015.

Ivo Danihelka, Greg Wayne, Benigno Uria, Nal Kalchbrenner, and Alex Graves. Associative long short-term memory. *arXiv preprint arXiv:1602.03032*, 2016.

Scott Wisdom, Thomas Powers, John Hershey, Jonathan Le Roux, and Les Atlas. Full-capacity unitary recurrent neural networks. In *Advances in Neural Information Processing Systems*, pages 4880–4888, 2016.

Sepp Hochreiter and Jürgen Schmidhuber. Long short-term memory. *Neural computation*, 9(8):1735–1780, 1997.

Tony A Plate. Holographic reduced representation: Distributed representation for cognitive structures. 2003.

David P Reichert and Thomas Serre. Neuronal synchrony in complex-valued deep networks. *arXiv preprint arXiv:1312.6115*, 2013.

Aaron van den Oord, Nal Kalchbrenner, Lasse Espeholt, Oriol Vinyals, Alex Graves, et al. Conditional image generation with pixelcnn decoders. In *Advances In Neural Information Processing Systems*, pages 4790–4798, 2016a.

Aäron van den Oord, Sander Dieleman, Heiga Zen, Karen Simonyan, Oriol Vinyals, Alex Graves, Nal Kalchbrenner, Andrew Senior, and Koray Kavukcuoglu. Wavenet: A generative model for raw audio. *CoRR abs/1609.03499*, 2016b.

Kyunghyun Cho, Bart Van Merriënboer, Dzmitry Bahdanau, and Yoshua Bengio. On the properties of neural machine translation: Encoder-decoder approaches. *arXiv preprint arXiv:1409.1259*, 2014.

Julian Georg Zilly, Rupesh Kumar Srivastava, Jan Koutník, and Jürgen Schmidhuber. Recurrent highway networks. *arXiv preprint arXiv:1607.03474*, 2016.

Guangji Shi, Maryam Modir Shanechi, and Parham Aarabi. On the importance of phase in human speech recognition. *IEEE transactions on audio, speech, and language processing*, 14(5):1867–1874, 2006.

Alan V Oppenheim and Jae S Lim. The importance of phase in signals. *Proceedings of the IEEE*, 69(5):529–541, 1981.

Oren Rippel, Jasper Snoek, and Ryan P Adams. Spectral representations for convolutional neural networks. In *Advances in Neural Information Processing Systems*, pages 2449–2457, 2015.

George M Georgiou and Cris Koutsougeras. Complex domain backpropagation. *IEEE transactions on Circuits and systems II: analog and digital signal processing*, 39(5):330–334, 1992.

Richard S Zemel, Christopher KI Williams, and Michael C Mozer. Lending direction to neural networks. *Neural Networks*, 8(4):503–512, 1995.

Taehwan Kim and Tülay Adalı. Approximation by fully complex multilayer perceptrons. *Neural computation*, 15(7):1641–1666, 2003.

Akira Hirose. *Complex-valued neural networks: theories and applications*, volume 5. World Scientific, 2003.

Tohru Nitta. Orthogonality of decision boundaries in complex-valued neural networks. *Neural Computation*, 16(1):73–97, 2004.

Geoffrey E Hinton, Simon Osindero, and Yee-Whye Teh. A fast learning algorithm for deep belief nets. *Neural computation*, 18(7):1527–1554, 2006.

Yoshua Bengio, Pascal Lamblin, Dan Popovici, Hugo Larochelle, et al. Greedy layer-wise training of deep networks. *Advances in neural information processing systems*, 19:153, 2007.

Christopher Poultney, Sumit Chopra, Yann L Cun, et al. Efficient learning of sparse representations with an energy-based model. In *Advances in neural information processing systems*, pages 1137–1144, 2007.

Joan Bruna, Soumith Chintala, Yann LeCun, Serkan Piantino, Arthur Szlam, and Mark Tygert. A mathematical motivation for complex-valued convolutional networks. *arXiv preprint arXiv:1503.03438*, 2015.

Edouard Oyallon and Stéphane Mallat. Deep roto-translation scattering for object classification. In *Proceedings of the IEEE Conference on Computer Vision and Pattern Recognition*, pages 2865–2873, 2015.

Mark Tygert, Arthur Szlam, Soumith Chintala, Marc’Aurelio Ranzato, Yuandong Tian, and Wojciech Zaremba. Scale-invariant learning and convolutional networks. *arXiv preprint arXiv:1506.08230*, 2015.

Michael Cogswell, Faruk Ahmed, Ross Girshick, Larry Zitnick, and Dhruv Batra. Reducing overfitting in deep networks by decorrelating representations. *arXiv preprint arXiv:1511.06068*, 2015.

Nitish Srivastava, Geoffrey E Hinton, Alex Krizhevsky, Ilya Sutskever, and Ruslan Salakhutdinov. Dropout: a simple way to prevent neural networks from overfitting. *Journal of Machine Learning Research*, 15(1):1929–1958, 2014.

Xavier Glorot and Yoshua Bengio. Understanding the difficulty of training deep feedforward neural networks. In *Aistats*, volume 9, pages 249–256, 2010.

Kaiming He, Xiangyu Zhang, Shaoqing Ren, and Jian Sun. Delving deep into rectifiers: Surpassing human-level performance on imagenet classification. In *Proceedings of the IEEE international conference on computer vision*, pages 1026–1034, 2015b.

Jonathan Tompson, Ross Goroshin, Arjun Jain, Yann LeCun, and Christoph Bregler. Efficient object localization using convolutional networks. In *Proceedings of the IEEE Conference on Computer Vision and Pattern Recognition*, pages 648–656, 2015.

Yurii Nesterov. A method of solving a convex programming problem with convergence rate $o(1/k^2)$. 1983.

Sergey Zagoruyko and Nikos Komodakis. Wide residual networks. *arXiv preprint arXiv:1605.07146*, 2016.

John Thickstun, Zaid Harchaoui, and Sham Kakade. Learning features of music from scratch. In *Proc. ICLR*, 2016.

Julius O Smith. Digital audio resampling. *Online* <http://www-ccrma.stanford.edu/~jos/resample>, 2002.

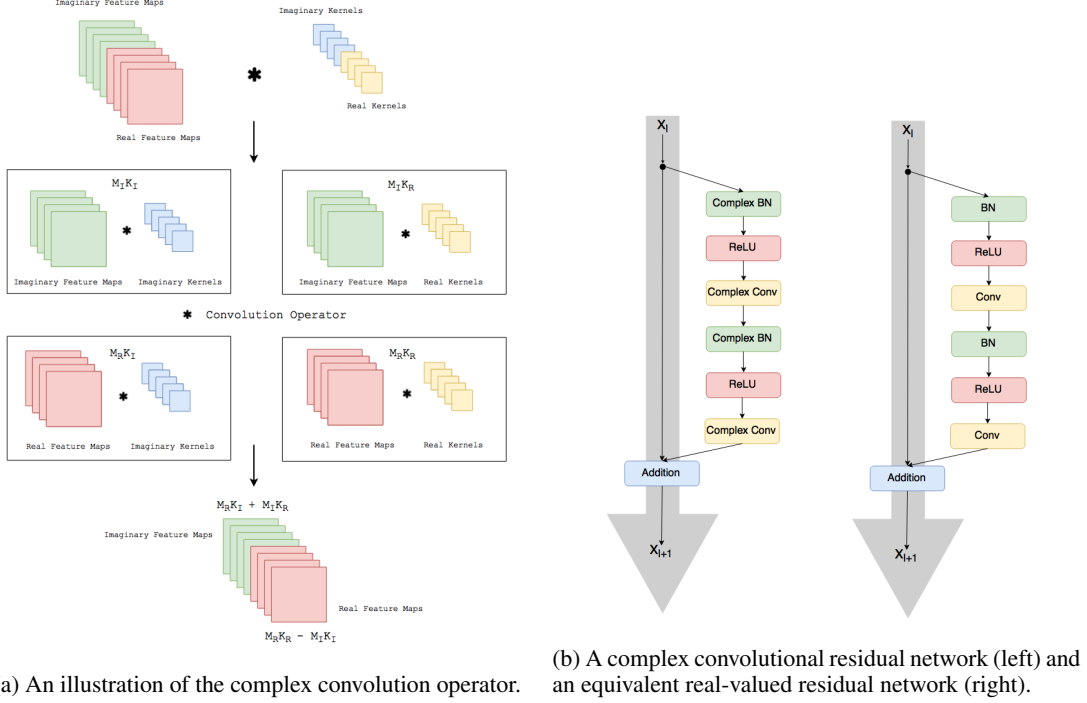
Karen Simonyan and Andrew Zisserman. Very deep convolutional networks for large-scale image recognition. In *Proc. ICLR*, 2015.

Theano Development Team. Theano: A Python framework for fast computation of mathematical expressions. *arXiv e-prints*, abs/1605.02688, May 2016. URL <http://arxiv.org/abs/1605.02688>.

François Chollet et al. Keras: Deep learning library for theano and tensorflow. *URL: https://keras.io/k*, 2015.

Appendix

In practice, the complex convolution operation is implemented as illustrated in Fig.1a where M_I , M_R refer to imaginary and real feature maps and K_I and K_R refer to imaginary and real kernels. $M_I K_I$ refers to result of a real-valued convolution between the imaginary kernels K_I and the imaginary feature maps M_I .



(a) An illustration of the complex convolution operator.

(b) A complex convolutional residual network (left) and an equivalent real-valued residual network (right).

Figure 1: Complex convolution and residual network implementation details.

Visualizations

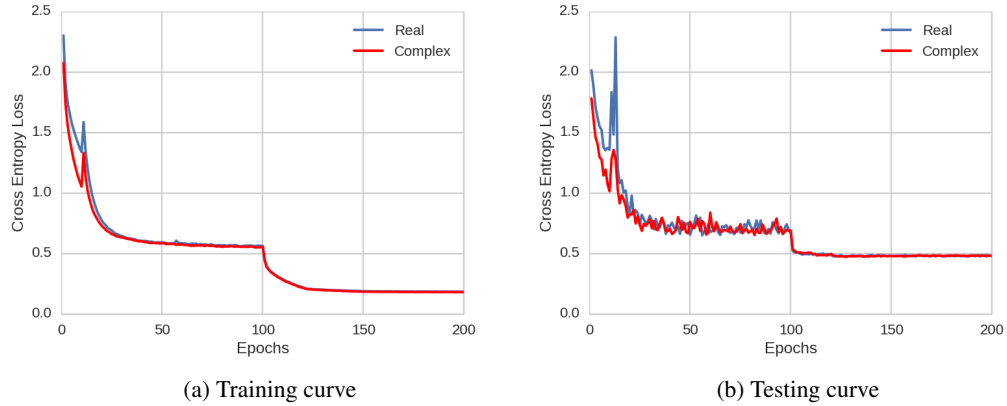


Figure 2: Training and test error curves for the small complex vs real valued network on CIFAR-10

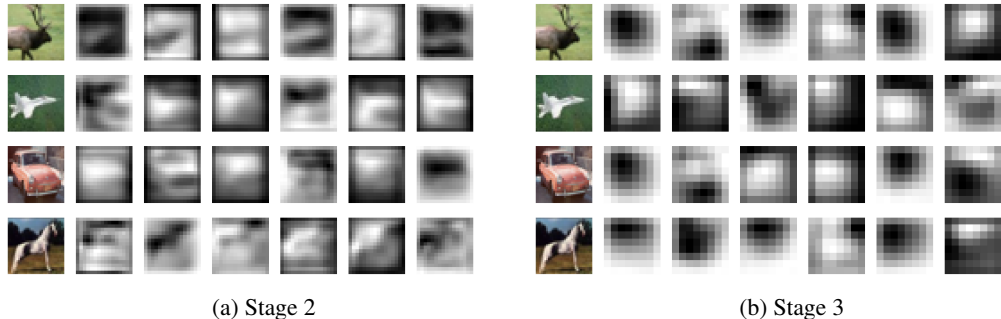
Figures 3 and 4 were generated using the small complex resnet model trained on CIFAR-10.



(a) Feature Maps

(b) Polar representation

Figure 3: (a) Stage 1 feature maps as real and imaginary pairs for each input, vs. (b) feature maps as magnitude and phase.



(a) Stage 2

(b) Stage 3

Figure 4: Stage 2 and 3 feature maps as real and imaginary pairs for each input

MusicNet illustrations

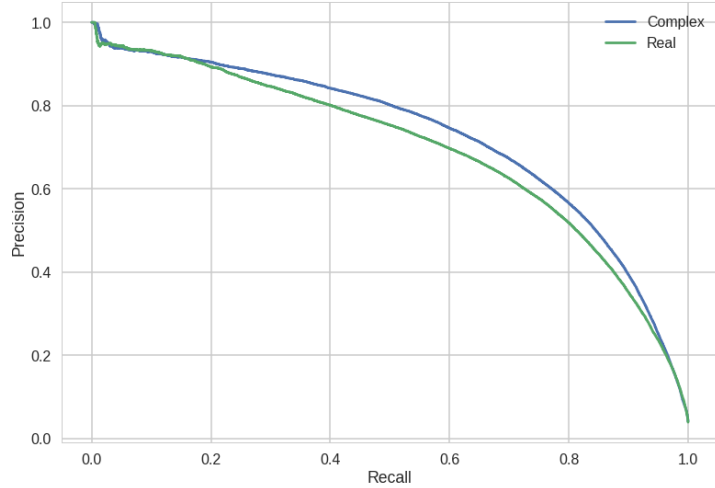


Figure 5: Precision-recall curve

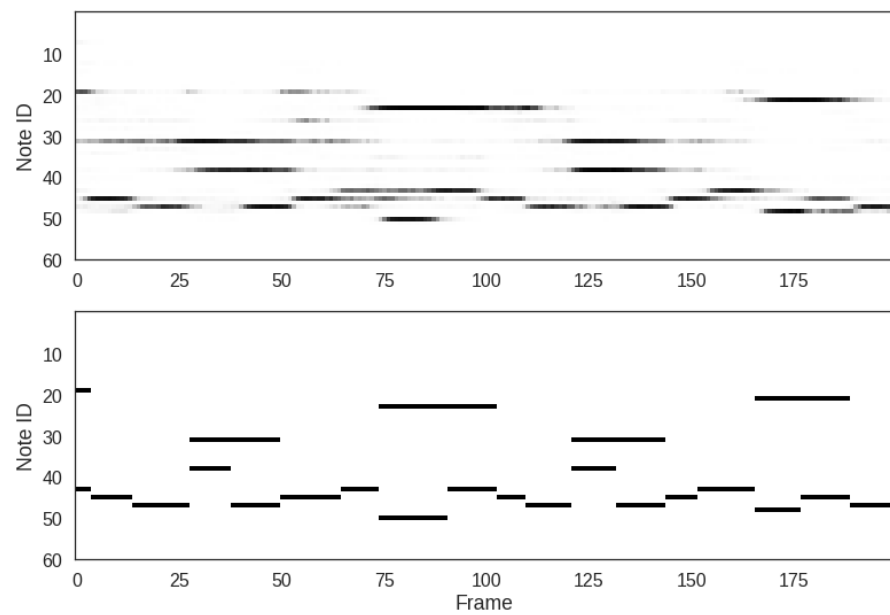


Figure 6: Predictions (Top) vs. ground truth (Bottom) for a music segment from the test set.